WORKING PAPER 96/6

COMPUTER SIMULATION OF RIVER CHANNEL DEGRADATION

A.P. Nicholas

PUBLISHED MAY 1996

For further copies contact the Working Paper Secretary,
School of Geography, University of Leeds, Leeds, LS2 9JT
Telephone 0113 233 3300

ABSTRACT

A theoretical model is presented that simulates the impact of a phase of bed degradation upon a straight channel with a gravel bed and cohesive banks. The model predicts the lateral distributions of flow depth, velocity and bed shear stress across a channel section for an imposed formative discharge. Downstream bedload transport rates are calculated as a function of local stream power and are employed to determine rates of bed degradation. A simple cross-stream transport model is used to predict the lateral redistribution of bed sediment. Bank retreat occurs by instability, block failure and deposition of failed bank material, for both cohesive and uncohesive sediments. Analysis of model output shows that model parameters can be divided into two subsets. Cohesive bank failure magnitude-frequency relationships are controlled largely by the properties of the bank material and the geometry of the bank and failure block. In contrast, the configuration of the gravel bed and the temporal sequence of bank failure, deposition of slump material and removal of sediment from the bank toe are controlled predominantly by factors which influence the relative rates of bed degradation and cross-stream sediment transport.

INTRODUCTION

River channel degradation results from an imbalance between the volumes of sediment entering and leaving a channel section. A stable river may therefore experience a phase of bed degradation as a result of either a reduction in sediment supply or an increase in local transport capacity. A channel disturbed in this way will respond by eroding its bed and banks until such time as a new equilibrium is established between sediment transport and supply rates (Schumm, 1969). Gradual but progressive river degradation (i.e. a few millimetres a year over hundreds or thousands of years) may result from the influence of long-term climate and land use changes upon drainage basin hydrology and sediment production (Knox,1983; Burrin, 1985) or from the steepening of river long profiles promoted by tectonic uplift, coastal erosion or changes in sea level (Leckie, 1994). Over historic and contemporary time-scales, human impacts upon water and sediment supply to rivers have led to more dramatic rates of channel degradation (Hickin, 1983; Lewin *et al.*, 1988). Channel incision and widening may be caused by increased river discharges resulting from catchment urbanisation (Park, 1977; Whitlow and Gregory, 1989). Alternatively, cross-section degradation may be promoted by increased channel slopes following river channelisation (Brookes, 1985; Erskine, 1992) or reduced sediment supply from upstream as a result of reservoir construction (Petts, 1979; Rasid, 1979). Erosion of channel bed and banks also occurs as part of the cycle of aggradation and degradation associated with the passage of large-scale sediment slugs in river systems (Nicholas *et al.*, 1995). For example, tin mining in the Ringarooma basin, Tasmania generated a wave of sedimentation that caused bed levels to fluctuate by 10 m over a 110 year period (Knighton, 1989). Maximum rates of bed incision over this time were approximately 0.5 m $year^{-1}$.

A considerable amount of qualitative work has been carried out into the causes and mechanisms of channel degradation. However, comparatively little theoretical modelling has been undertaken to enable quantitative analysis of the factors controlling fluvial erosion processes. This paper describes a model that simulates the response of straight river channels to a phase of bed degradation. Figure 1 shows a

flow chart illustrating the important process-form interrelationships controlling the evolution of degrading straight channel sections. This flow chart also serves to outline the links between the main components of the numerical model presented below. The lateral distributions of flow depth, velocity and stream power are controlled by the shape of the cross-section, the channel bed slope and roughness, and the discharge entering the section. Stream power controls the local downstream sediment transport capacity which is balanced against the sediment entering the section from upstream to determine the rate at which the channel bed is lowered. At the base of the bank, vertical lowering of the bed may be accompanied by a degree of lateral bank trimming. Cross-stream sediment transport promotes the removal of material that has accumulated at the bank toe. Vertical and lateral displacement of the bank toe, resulting from bed scour and cross-stream sediment redistribution, lead to an increase in bank height and steepness. These changes in geometry may result in the bank becoming unstable. When this occurs the bank fails and sediment is deposited at the bank toe. This slumped material protects the bank from further failures until it is removed either by lateral redistribution driven by cross-stream sediment transport or by net removal of material from the section (i.e. removal in a downstream direction).

MODEL OUTLINE

Relatively few models of bed degradation and bank erosion are reported in the literature. Pickup (1976) and Mosselman (1992) present treatments of degradation processes for channels with simplified geometries. Pizzuto (1990) derives a model of river widening for channels with uncohesive beds and banks. He combines representations of cross-stream gravel transport and planar bank failure to predict equilibrium channel bank profiles. Osman and Thorne (1988) present an analysis of the stability of cohesive river banks. They employ this stability analysis, in conjunction with a simple bed degradation model, to examine changes in channel dimensions promoted by incision downstream of a dam (Thorne and Osman, 1988).

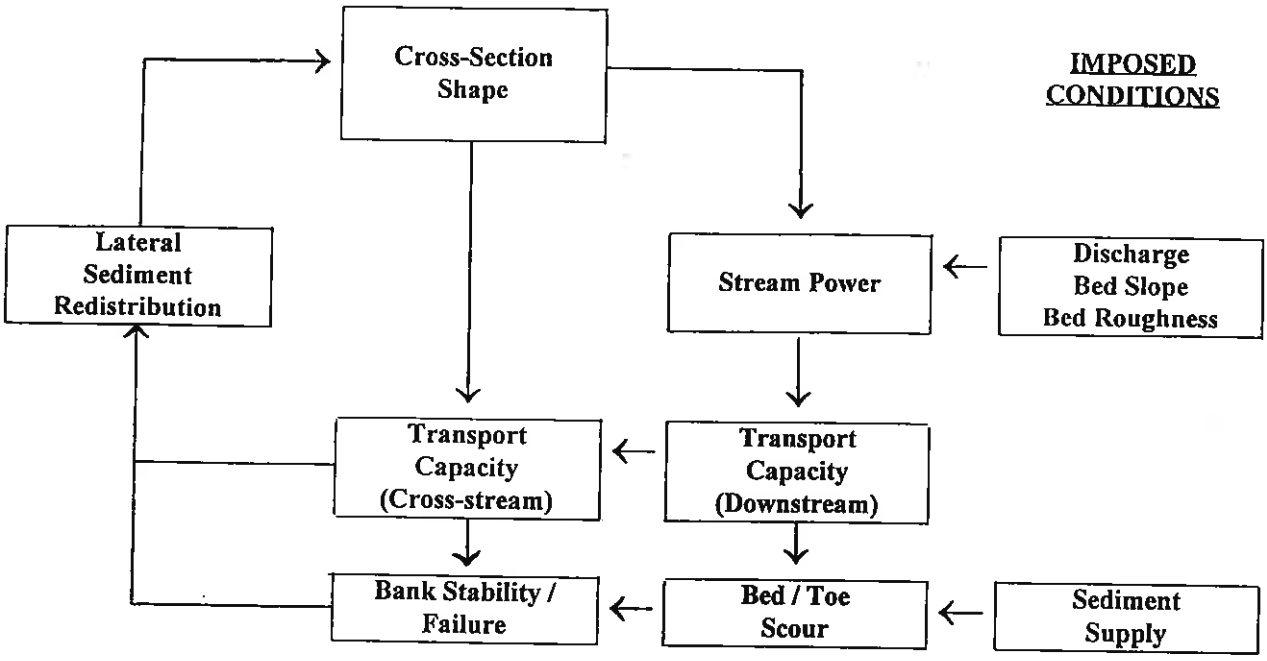

Figure 1: Flow chart outlining the important process-form interrelationships controlling the evolution of straight degrading channel sections.

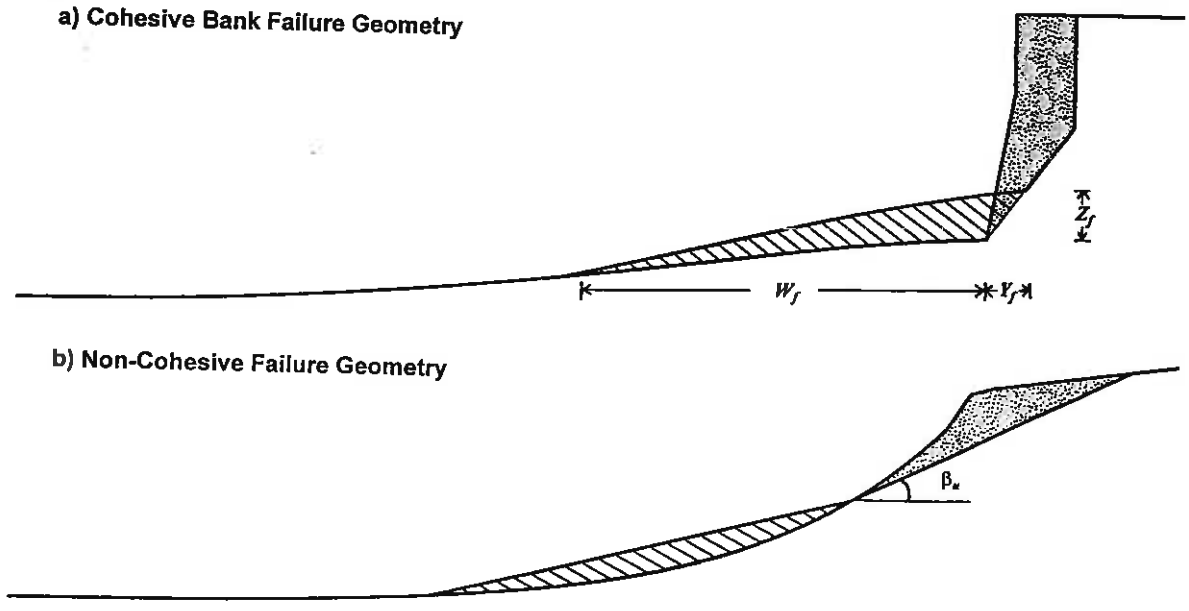

Figure 2: Model representations of; a) cohesive bank failure geometry; and b) non-cohesive failure geometry.

The model presented here addresses the degradation of channels with cohesive banks and gravel beds. As such it is widely applicable to British rivers. The bed degradation model of Thorne and Osman (1988) also deals with channels of this type, however, the current scheme differs considerably from their model in its representation of cross-stream sediment transport and the redistribution of material deposited as a result of bank failure. Thorne and Osman employ a 1D sediment routing scheme to balance sediment fluxes in a series of channel cross-sections characterised by flat beds. In their model, when a bank failure occurs the sediment supplied to the channel does not accumulate at the toe of the bank and alter the section geometry. Instead, the time taken to remove the deposited bank material is determined from the difference between sediment supply and transport rates at the section. During this time period, termed the basal clean-out phase, no further bed degradation occurs at the section. The model presented here is intended to address the sequence of bank instability, failure and basal clean-out in greater detail. The channel cross-section is divided into two components; the gravel bed and the cohesive bank. The gravel bed is sub-divided into approximately 200 elements of equal width for the purpose of determining lateral distributions of hydraulic variables and bedload transport rates. The cohesive bank is defined by an inclined lower portion, a vertical upper portion and a flat floodplain surface. The bank is assumed to be composed of a range of particle sizes including clay, silt, sand and gravel. The link between the cohesive bank and the gravel bed is termed the bank toe. When a failure occurs the dimensions of the cohesive bank are redefined and the failure block is deposited as a wedge of slumped material covering the toe of the bank. Basal clean-out then proceeds by a combination of bed scour due to net sediment removal from the cross-section and lateral sediment redistribution promoted by the cross-stream component of bedload transport.

The model aims to simulate channel incision and widening in response to rapid or substantial bed degradation. In such situations, concentrated scour in the centre of the bed may promote the development of a significant cross-stream gravel slope. In order to cope with this phenomenon the model also incorporates a simple treatment of non-cohesive sediment failures based upon that of Pizzuto (1990).

Model representations of both cohesive and non-cohesive failure mechanisms are shown in Figure 2, and examined in greater detail below.

The model runs through a series of time steps as the initial cross-section shape evolves towards a final equilibrium form in response to a phase of bed degradation. At the start of each time step the lateral distributions of flow depth, velocity and bed shear stress are determined across the section. In its current form the model employs a single formative discharge rather than a flow-frequency distribution. This formative or dominant discharge is set equal to the bankfull discharge for the initial channel form (i.e. at the start of the simulation). Hydraulic calculations proceed by estimating the height of the water surface, calculating the resulting discharge and then employing Newton-Raphson iteration to determine an improved water surface estimate. This procedure continues until the correct water surface level is obtained.

As identified above, the gravel bed is divided into 200 elements or nodes. For the purpose of carrying out hydraulic calculations, additional nodes are located at equal spaces along the inclined portion of the cohesive bank. The boundary shear stress (τ) at each node across the channel is given by the depth-averaged momentum equation for steady uniform flow in a downstream direction (Shiono and Knight, 1991)

$$\tau \ (1+S_y^2)^{0.5} = \rho g h S_o + \frac{\partial (h\tau_{yx})}{\partial y} \tag{1}$$

where ρ is the fluid density, g is acceleration due to gravity, S_o is the downstream channel bed slope, S_y is the cross-stream bed slope, h is the flow depth, y is the cross-stream coordinate and τ_{yx} is the depth-averaged transverse shear stress. Equation (1) neglects secondary flows and is valid only where bed curvature is low (Parker, 1978; Pizzuto, 1990).

The depth-averaged transverse shear stress is determined using the eddy viscosity approach

$$\tau_{yx} = \rho \varepsilon \frac{\partial U}{\partial y} \tag{2}$$

$$\varepsilon = \lambda U_* h \tag{3}$$

where ε is the eddy viscosity, λ is a dimensionless eddy viscosity coefficient, and U and U_* are the downstream velocity and shear velocity respectively. The velocity, shear velocity and boundary shear stress are related by the following expressions

$$U = (8/f)^{0.5} U_* \tag{4}$$

$$(1/f)^{0.5} = m(h/D_{50})^c \tag{5}$$

$$U_* = (\tau / \rho)^{0.5} \tag{6}$$

where f is the Darcy-Weisbach friction factor, D_{50} is the 50th percentile of the bed sediment and m and c are empirical coefficients. Equation (5) is a power law approximation of a Keulegan-type logarithmic resistance law (Ferguson, 1994). By substituting (2) and (3) into the second term on the right hand side of (1), using (4)-(6) to replace velocities and shear velocities by boundary shear stresses, and neglecting small-scale variations in relative roughness between adjacent bed nodes equation (1) can be simplified to

$$\tau(1+S_y^2)^{0.5} = \rho g h S_o + m\lambda\sqrt{2} D_{50}^{-c} \frac{\partial}{\partial y}\left(h^{2+c} \frac{\partial \tau}{\partial y} \right) \tag{7}$$

Expressing this relation in finite difference form generates a series of n simultaneous linear equations which yield a tridiagonal matrix. The cross-section is assumed to be symmetrical so that calculations are necessary on only one side of the channel centreline. Suitable boundary conditions for solving equation (7) are

$$\tau = 0 \qquad y = W/2 \tag{8}$$

$$\frac{\partial \tau}{\partial y} = 0 \qquad y = 0 \tag{9}$$

where $W/2$ is the channel bed half-width (i.e. the distance from the centreline to the bank toe).

The lateral distribution of downstream sediment transport rates is calculated using a modified version of Bagnold's stream power relation (Bagnold, 1980)

$$qs = qs_r (\omega / \omega_r)^{1.5} (h/h_r)^{-0.67} (D_{50}/D_{50r})^{-0.5} \tag{10}$$

$$\omega = U\tau \tag{11}$$

where qs is the downstream sediment transport rate per unit width, ω is the stream power and qs_r, ω_r, h_r and D_{50r} are reference values of the transport rate, stream power, flow depth and bed D_{50}. The parameters h_r and D_{50r} were assigned values of 0.1 m

and 0.0011 m respectively after Bagnold (1980). Considerable uncertainty surrounds the specification of a suitable entrainment threshold for use in bedload transport relations. Parker (1990) presents a transport function that includes no entrainment threshold, so that transport rates approach zero only at very low shear velocities. A similar approach is adopted here using a reference stream power that is a function of the ratio of the bed sediment size to the fluid depth-slope product

$$\omega_r = A^B \tag{12}$$

$$B = \frac{1}{\tau_* \gamma} \tag{13}$$

$$\tau_* = \frac{\tau}{(\rho_s - \rho) g D_{50}} \tag{14}$$

$$\gamma = \frac{\rho_s - \rho}{\rho} \tag{15}$$

where ρ_s is the sediment density and τ_* is the dimensionless shear stress. The constant (A) in equation (12) was assigned a value of 1.015 by fitting the predictions of equation (10) to those generated using Bagnold's original formula.

Temporal changes in bed elevation may be related to downstream variations in sediment transport rates at a series of channel cross-sections using the sediment continuity equation

$$W \frac{\partial z}{\partial t} = -\frac{1}{(1-X)} \frac{\partial Qs}{\partial x} \tag{16}$$

where z is bed elevation, t is time, Qs is the width integrated downstream transport rate, x is the downstream coordinate and X is the porosity of the bed sediment.

The performance of the model presented here is examined in the context of morphological changes at a single cross-section. In order to do this temporal variations in rates of erosion at the section (i.e. the left hand side of equation (16)) are specified. A phase of bed degradation is simulated during which rates of sediment removal from the section decline over time in an exponential fashion. This represents just one of many possible channel evolution scenarios (c.f. Schumm and Lichty, 1965; Graf, 1977)

$$A_e = A_E (1 - e^{\Gamma t}) \tag{17}$$

where A_e is the net area of erosion from the section up to time t, A_E is the total area of erosion during the phase of bed degradation and Γ is a decay constant. The model employs a time step (Δt) that varies in length depending upon the rate of bed degradation. During a single time step, an erosion increment (ΔA_e) is removed from the cross-section

$$\Delta A_e = \Delta A_b + \Delta A_l \tag{18}$$

where ΔA_b and ΔA_l represent bed degradation and lateral bank toe scour respectively. Net erosion is distributed between bed and bank toe elements by calculating the area of lateral toe scour and assuming that the remaining sediment is removed from the bed. Lateral bank retreat rates may be predicted independently of bed degradation as a function of excess shear stress (Arulanandan *et al.*, 1980). However, the objective here is to distribute total channel erosion between its horizontal and vertical components. In order to do this the rate at which the bank toe retreats is determined as a simple function of the rate of total channel erosion, the depth of near bank flow and the geometry of the bank

$$\Delta A_l = \Delta A_e \left(\frac{G}{1+G} \right) \tag{19}$$

$$G = \frac{\mu \, h_b}{W/2} (1 - 0.5/S_l) \tag{20}$$

where h_b is the depth of flow at the toe of the bank, S_l is the lateral slope of the inclined lower portion of the bank and μ is an empirical coefficient. The bed degradation increment is distributed by assuming that the depth of bed incision at each channel node is proportional to the downstream sediment transport capacity determined from equation (10). This approach has been adopted previously by Chang (1982) and others (c.f. Dawdy and Vanoni, 1986).

Rates of lateral sediment transport are calculated using a simplified version of the cross-stream bedload transport model of Kikkawa *et al.* (1976) and Parker (1983). Pizzuto (1990) expresses this lateral sediment transport scheme in the form

$$ql = qs \left(\frac{1 + \alpha \tan \beta_u}{\tan \beta_u} \right) \left(\frac{\tau_{*c}}{\tau_*} \right)^{0.5} \frac{\partial z}{\partial y} \tag{21}$$

where ql is the cross-stream sediment transport rate, α is the ratio of lift to drag, β_u is the angle of repose of the bed sediment and τ_{*c} is the critical dimensionless shear

stress for sediment entrainment. In this study equation (21) is simplified by replacing the parameters α, β_u, τ_{*c}, ρ_s and ρ by a single coefficient (E_l). By doing this (21) is reduced to

$$ql = qs\ E_l B^{0.5} \frac{\partial z}{\partial y} \tag{22}$$

Temporal changes in bed elevation resulting from lateral redistribution of bed sediment are determined from equation (22) coupled with the cross-stream sediment continuity equation

$$\frac{\partial z}{\partial t} = -\frac{1}{(1-X)} \frac{\partial ql}{\partial y} \tag{23}$$

Vertical and horizontal erosion of the bank toe (see Figure 3a) result in increases in bank height and steepness. During each time step a Thorne and Osman (1988) type stability analysis is carried out on the cohesive bank to establish the timing of bank failures. Figure 3b shows the geometry of the cohesive bank before and after the occurrence of a failure. It should be noted that the geometry of the bank and failure block, and the representation of erosion of the bank toe during the period between failures, differ from those employed by Thorne and Osman (1988). The bank is assumed to fail at a constant angle (β). Horizontal and vertical erosion of the bank toe cause the bank angle to increase over time, so that immediately prior to the next failure the bank is inclined at an angle (i). The stability of the bank is determined from a factor of safety (FS)

$$FS = F_R / F_D \tag{24}$$

where F_R and F_D are the forces resisting and driving the failure.

$$F_R = C\,l + Wt\ \cos\beta\ \tan\phi \tag{25}$$

$$F_D = Wt\ \sin\beta \tag{26}$$

where C and ϕ are the bank material cohesion and angle of friction respectively, l is the length of the inclined portion of the failure block and Wt is the weight of the failure block given by

$$Wt = A_B \theta \tag{27}$$

$$A_B = 0.5(y_1(d-d_o) + y_2(H+d)) \tag{28}$$

a) Vertical and Horizontal Erosion of Bank Toe

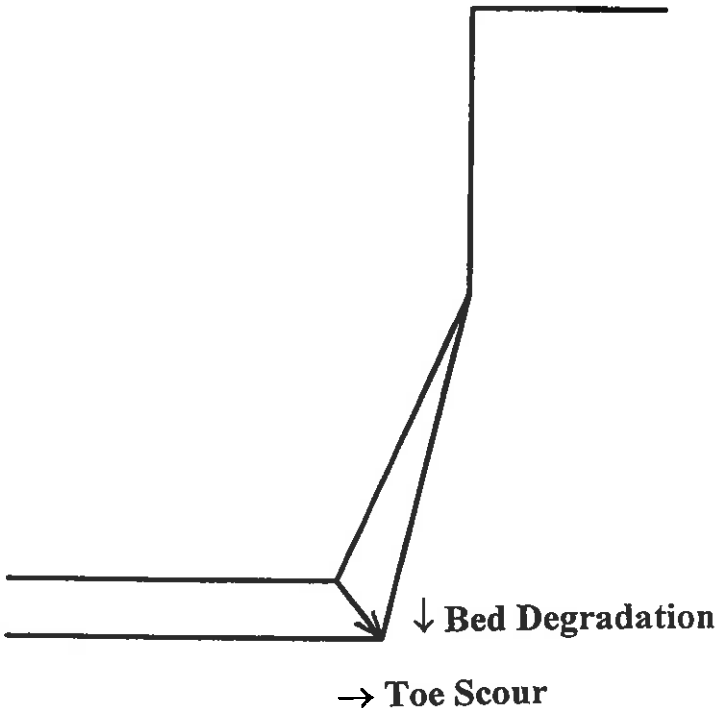

b) Bank Stability Analysis

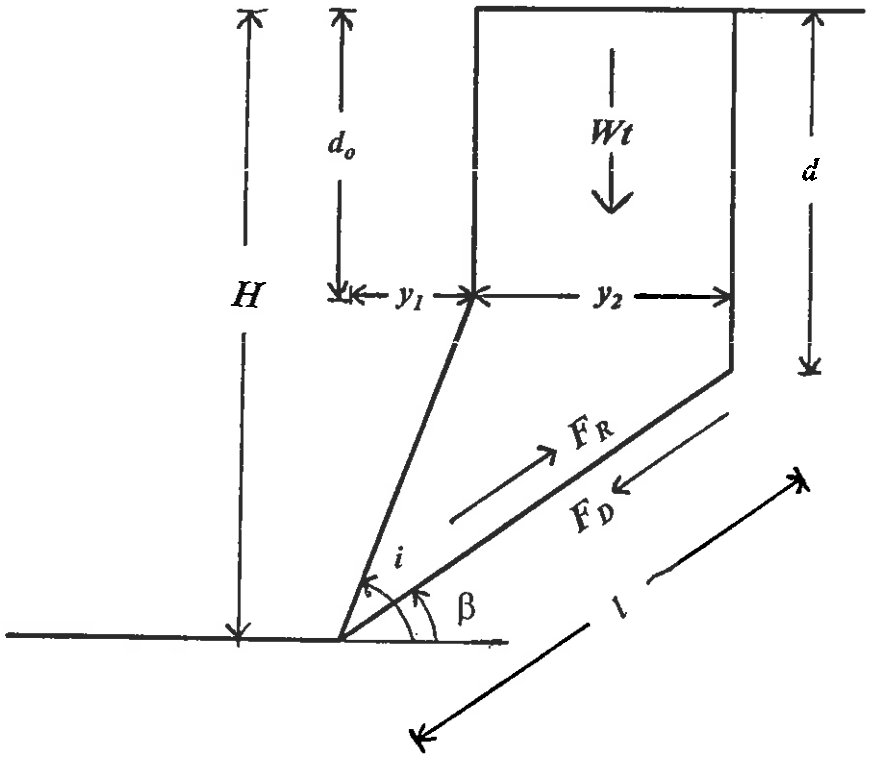

Figure 3: Model representations of; a) vertical and horizontal erosion of the bank toe; and b) cohesive bank stability analysis.

where θ is the unit weight of the bank material, A_B is the area of the failure block and the other terms in equation (28) are the geometric properties of the bank and failure block shown in Figure 3b and given by

$$d = KH \tag{29}$$

$$l = (H - d) / \sin\beta \tag{30}$$

$$y_1 = (H - d_o) / \tan i \tag{31}$$

$$y_1 + y_2 = (H - d) / \tan\beta \tag{32}$$

where d and d_o are the depths of the current and previous tension cracks respectively. Tension crack depths are related to bank height by the empirical coefficient K. Thorne and Abt (1993) suggest that K should take a value between 0.3 and 0.7.

Bank failure occurs when the factor of safety falls below 1. When this happens the dimensions of the cohesive bank are redefined and the failed bank material is deposited as a wedge of sediment covering the bank toe. The toe deposit is assumed to have a simplified geometry (shown in Figure 2a) that is described by

$$L_f = Y_f + W_f \tag{33}$$

$$W_f = r\left(\frac{W}{2}\right) \tag{34}$$

$$Y_f = r(y_1 + y_2) \tag{35}$$

$$Z_f = r(H - d) \tag{36}$$

where r is an index of the magnitude of the failure that takes a value between 0 and 1. Depths of deposited material are assumed to vary linearly with horizontal distance on either side of the bank toe

$$d_f = Z_f\left(1 - \frac{L}{L_f}\right) \qquad L > Y_f \tag{37}$$

$$d_f = Z_f\left(\frac{L}{Y_f} - \frac{L}{L_f}\right) \qquad L \le Y_f \tag{38}$$

where L is the horizontal distance measured from the point on the deposit closest to the cohesive bank towards the channel centreline. The area of the slump deposit (A_D) is related to the area of the failure block by

$$A_D = P\,A_B = 0.5\;Z_f\;W_f \tag{39}$$

where P is the proportion of the failure block that is deposited at the toe of the bank (as opposed to being removed immediately from the section in a downstream direction). By combining equations (33) to (39) the magnitude (r) of a given failure may be determined from

$$r = \left(\frac{4PA_B}{W(H-d)} \right)^{0.5} \tag{40}$$

The model also incorporates a simple treatment of gravel failures based upon the work of Pizzuto (1990) (see Figure 2b). Uncohesive sediment failures occur when the lateral slope of the gravel bed exceeds the tangent of the angle of repose of the sediment. Following Pizzuto (1990) the size of the failure block is determined by extending the plane of the failure upwards along a line at this critical angle. The mobilised gravel is deposited as a wedge with a linear surface that extends downslope of the point of failure. In the model, the lateral extent of gravel failures is limited to the toe of the cohesive bank. When the plane of a gravel failure reaches this point the cohesive bank is undermined and may also fail. This is an important mechanism of bank retreat where rates of bed degradation are rapid.

MODEL PERFORMANCE

The numerical model outlined above may be used to simulate the degradation of a series of connected channel sections by employing equation (16). In such simulations, morphological change at a cross-section will reflect not only the process-form feedbacks within the given section, but also downstream gradients in model variables (particularly bed slope and sediment transport rates). Before the model can be applied to field situations and tested in this manner, it is important that the interrelationships between model processes and the sensitivity of model behaviour to variations in parameter values are assessed at individual cross-sections. This can be achieved by employing equation (17) to simulate a phase of channel erosion in a controlled manner. This paper examines the performance of the numerical model in respect of such a degradation phase. All model simulations reported here were carried out using the same initial channel geometry; channel half width ($W/2$) = 20 m, channel

depth (D) = 2 m, height of vertical bank section (d_o = 1 m) and initial angle of inclined bank section (i) = 1.5 radians. In addition, the total area of erosion at the cross-section was also held constant throughout these simulations; channel erosion area (A_E) = 100 m^2. This area of erosion is representative of a phase of significant bed degradation and is of the same order as that reported by Knighton (1989). In the following sections, values of model variables during simulations are often given in dimensionless form

$$V^* = V_t / V_i \tag{41}$$

where V_t is the value of the variable at time t and V_i is the initial value of the variable. Table 1 shows the default parameter dataset employed in the model. Cohesive and uncohesive bank failure parameter values were obtained from the work of Osman and Thorne (1988) and Pizzuto (1990). Other parameters were assigned values within the realistic range of channel dimensions and properties. The parameter E represents the effectiveness of the cross-stream sediment transport. Because lateral variations in rates of bed degradation are controlled by relative, rather than absolute, variations in downstream sediment transport rates, the only impact of altering qs_r is on cross-stream sediment transport (through equation (22)). Hence, the effectiveness of cross-stream transport may be defined as

$$E = qs_r E_t \tag{42}$$

Parameter	Default	Maximum	Minimum	Unit
K	0.5	0.7	0.3	%
C	13	19	7	KN m^{-2}
θ	15.1	21	9	KN m^{-3}
P	1	1	0	%
β	0.785	1.16	0.41	radians
ϕ	0.1222	0.18	0.06	radians
β_u	0.5764	0.85	0.29	radians
μ	0.1	1	0.01	-
Γ	0.15	1.5	0.015	-
S_o	0.005	0.05	0.0005	-
D_{50}	0.05	0.09	0.01	m
λ	0.13	1.3	0.013	-
E	0.006	0.06	0.0006	%

Table 1: Model default parameter values.

An initial model run was carried out using the default parameter values. Channel adjustment took place over a period of 70 hours during this run. Given that the model employs a single formative discharge this time period may represent of the order of 1-10 years in real time. Variations in the length of the model simulations are controlled by the decay constant (Γ) in equation (17) and are addressed in a later section. Model simulations were concluded when the cross-section had attained a new equilibrium form, characterised by a flat channel bed (over which zero lateral sediment transport occurs) and a stable cohesive bank.

Figure 4a shows the changes in channel width and depth over the course of the simulation. Figure 5 shows the shape of the cross-section at four instants in time during the simulation. Initially, degradation of the channel bed is concentrated in the middle of the cross-section where stream power is greatest. Over time, positive feedbacks between bed incision, flow depth and stream power increase the lateral channel bed gradient (Figure 5, t = 5.1 hr). This promotes greater rates of cross-stream sediment transport. Vertical and horizontal displacement of the bank toe, caused by net removal of sediment from the section and lateral redistribution of sediment in the direction of the transverse bed slope, result in increases in bank height and steepness, and ultimately in bank failure. Following failure of the cohesive bank, sediment is deposited at the bank toe and bank stability is greatly increased (Figure 5, t = 5.3 hr). Basal clean-out then proceeds (Figure 5, t = 6.5 hr) and the bank factor of safety is gradually reduced towards the critical value when the next bank failure is imminent (Figure 5, t = 10 hr). Figure 4a shows channel width increasing in a series of steps each representing a bank failure. These failures can also be identified in the cycles of changing bank stability, indicated in Figure 4b by the factor of safety of the cohesive bank. The dimensionless channel centreline depth (D^*) is shown to increase rapidly to a maximum value of approximately 2.95 after 15 hours before declining over the rest of the simulation to a final value of 2.68. This reflects the concentration of incision in the middle of the channel and the creation of a significant cross-stream channel bed slope during the early stages of the simulation when degradation rates are high. As rates of erosion decline over time, the high cross-stream bed slope drives lateral sediment transport which seeks to redistribute the bed material and re-establish a flat, equilibrium channel bed.

a)

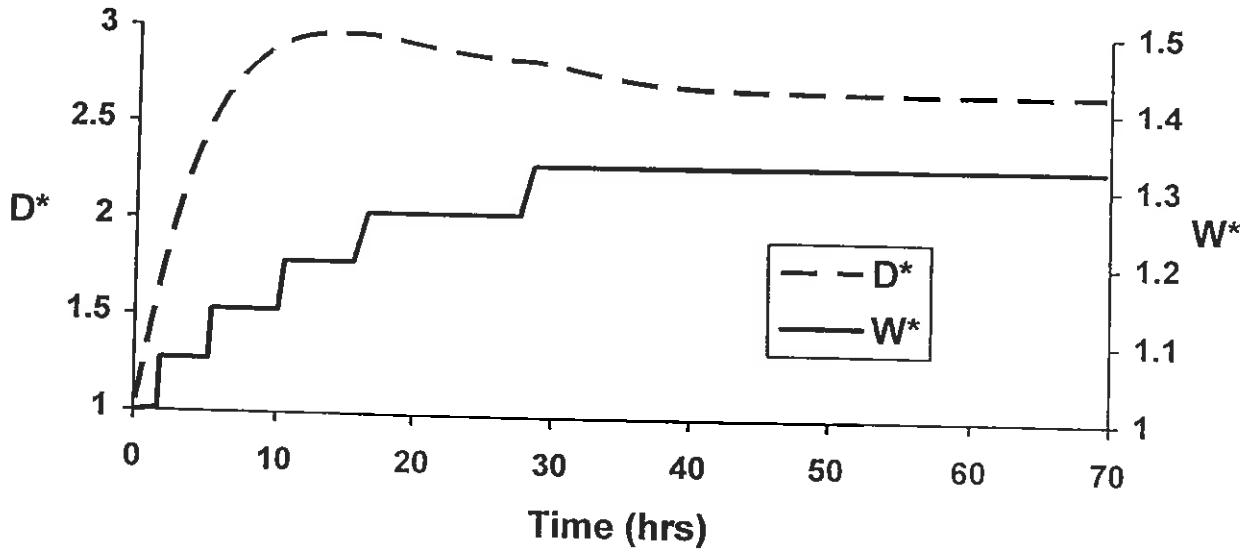

b)

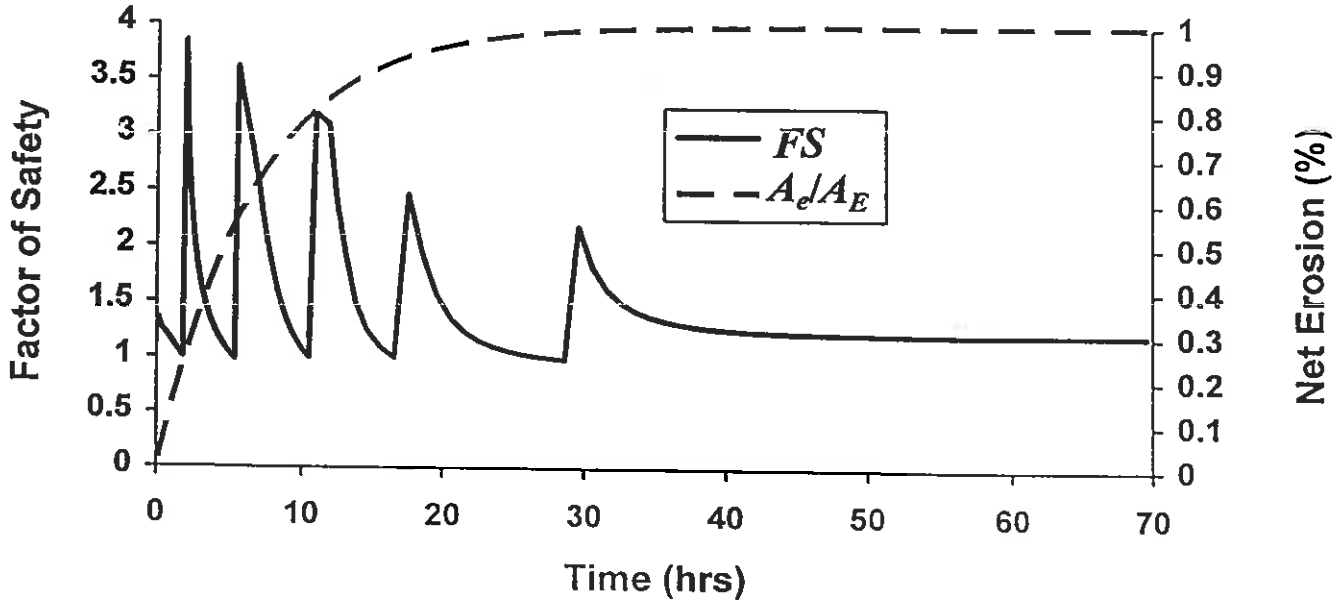

Figure 4: Model simulation results for the default parameter dataset; a) temporal variations in dimensionless channel width and depth; and b) temporal changes in bank stability and net channel erosion.

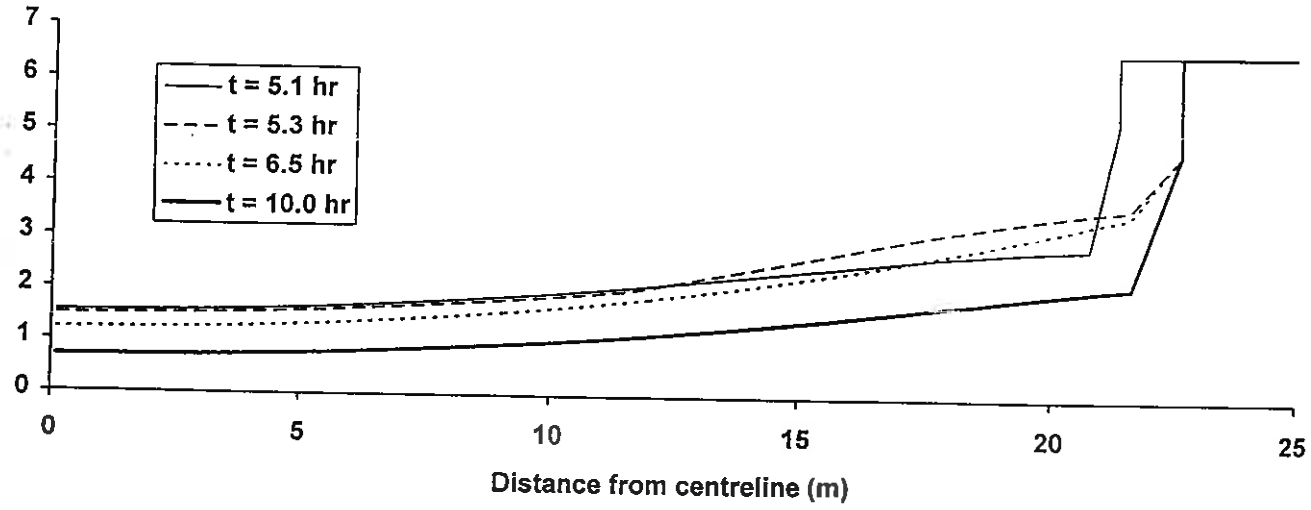

Figure 5: Simulated channel cross-sections for the model run based upon the default parameter dataset.

A series of simulations were conducted to examine the sensitivity of the model to variations in parameter values. Approximately 50 model runs were carried out with each parameter being varied across the range indicated in Table 1. A single parameter was adjusted at the start of each run. All other parameters were held at their default values. Figures 6a to 6c show the impact of variations in parameter values upon the number of cohesive bank failures, the mean magnitude of the failure blocks and the dimensionless ratio of net widening to deepening during model simulations. The dashed lines in these figures indicate the value of the dependent variable for the default parameter dataset. Maximum and minimum points relate to the maximum and minimum parameter values employed which are shown in Table 1. Varying the parameter values between these two extremes produced trends consistent with those shown in Figure 6a to 6c, however, trends were generally non-linear. Furthermore, the discontinuous nature of the bank failure mechanism results in relationships between parameter values and number of failures that exhibit thresholds rather than gradual transitions in failure frequency.

A number of patterns emerge from Figures 6a to 6c. Each of the aspects of the model performance examined appears to be more sensitive to the first five parameters in Table 1 (K, C, θ, P, and β) than the other eight. This is perhaps not surprising since these parameters control the weight and geometry of the failure block and the proportion of the failed material deposited at the bank toe. As one would expect, an inverse relationship is evident between bank failure mean magnitude and frequency. In addition, for the first four of these five parameters small high frequency bank failures were found to be on average 50 % more effective than large low frequency failures (where effectiveness is indicated by the product of number of failures and mean failure magnitude). Further comparison of Figures 6a and 6c shows that for all the parameters for which variations in the number of bank failures were recorded (except β) greater numbers of bank failures are associated with higher ratios of net widening to deepening, even though mean failure magnitude is reduced. In contrast to the other parameters, values of β both higher and lower than the default value lead to a reduction in the number of cohesive bank failures observed. The reason for this can be seen in equations (24) to (32). As β gets very low the component of the weight of the failure block driving instability declines relative to component resisting instability,

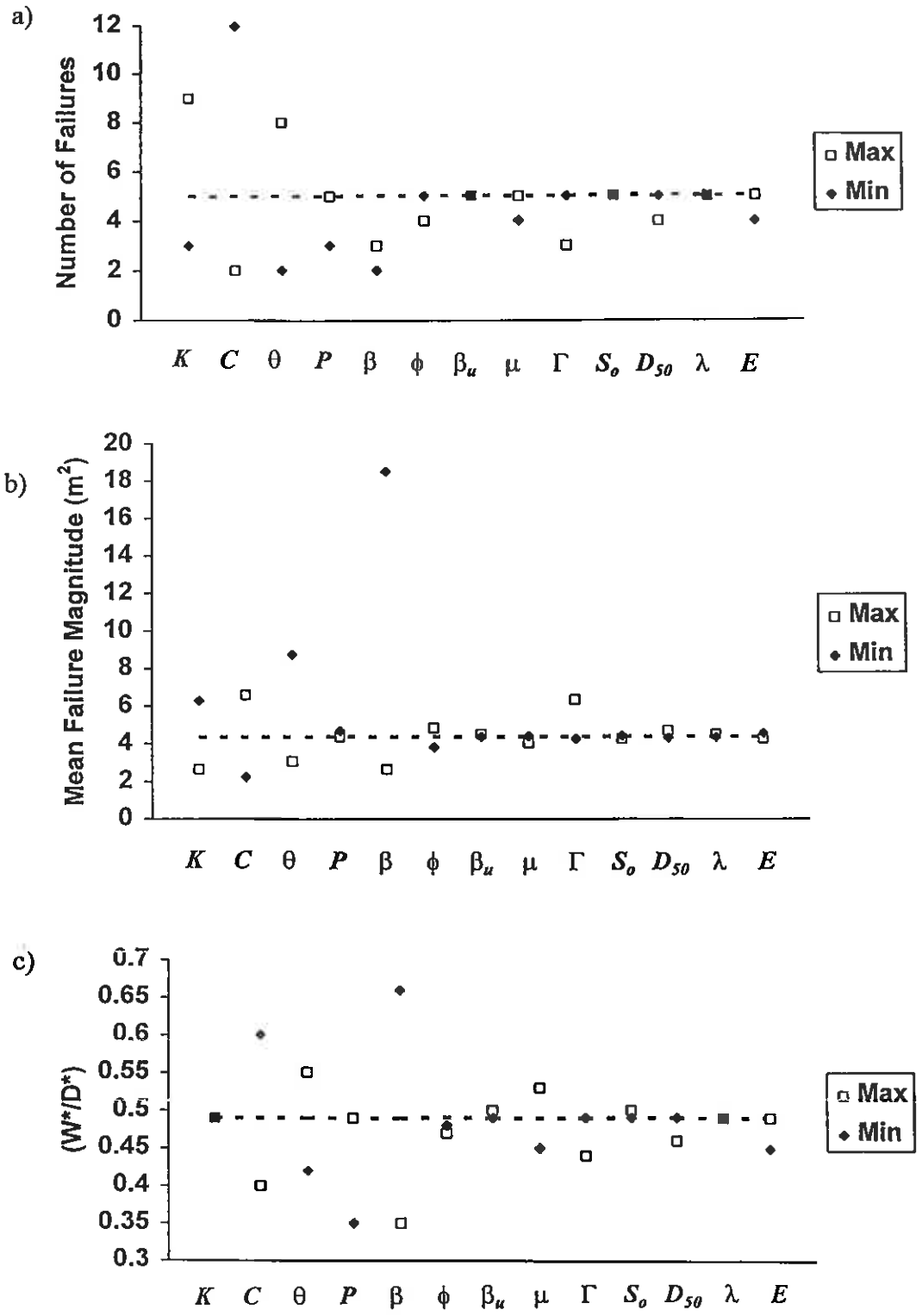

Figure 6: Sensitivity analysis showing the impact of variations in model parameter values upon; a) the number of cohesive bank failures during a simulation; b) the mean magnitude of bank failures during a simulation; and c) the ratio of the dimensionless rates of channel widening to deepening.

hence failures become less frequent. As β gets very large the reverse happens, however, as β approaches 90° the failure block gets smaller and so its weight decreases. As a result, although the second term on the right hand side of (25) approaches zero, the first term becomes large relative to the weight of the block driving instability, hence bank stability increases and again failures become less frequent. Clearly, an optimum bank angle exists at which bank stability is minimised and failure frequency is maximised. This angle, which represents that at which failures are most likely to occur, is identified by Osman and Thorne (1988). Osman and Thorne assume that following an initial bank failure at this critical angle, subsequent failures occur by parallel bank retreat. The model presented here is simplified in that the failure angle of the bank is specified initially. It is apparent that this angle is an important control on the magnitude and frequency of bank failures and that it should be assigned a value close to that for which bank stability is minimised.

In the previous section, changes in model parameter values were shown to influence the final equilibrium form of the cross-section (Figure 6c). The effectiveness of cross stream sediment transport (E) and the erosion decay constant (Γ) appear to be less important in this respect than the factors which control the dimensions and weight of the cohesive bank failure block. However, although changes in these two parameters may have little impact upon variations in final channel widths and depths, they exert a considerable influence on the evolution of channel morphology during simulations.

Figures 7, 8 and 9 show temporal variations in channel dimensions and sequences of channel cross-section shapes for three simulations involving different values of E. During these model runs other parameters were set at their default values. In these Figures, Ws^* is the dimensionless water surface width and SY is a multiple of the mean cross-stream channel bed slope (Sy)

$$SY = \Omega \; Sy \tag{44}$$

$$Sy = \frac{\Delta z}{(W/2)} \tag{45}$$

where Δz is the height difference between the toe of the cohesive bank and the channel bed at the centreline and Ω is a constant that is set equal to 10 so as to bring values of SY within a suitable range for plotting in Figures 7 to 9.

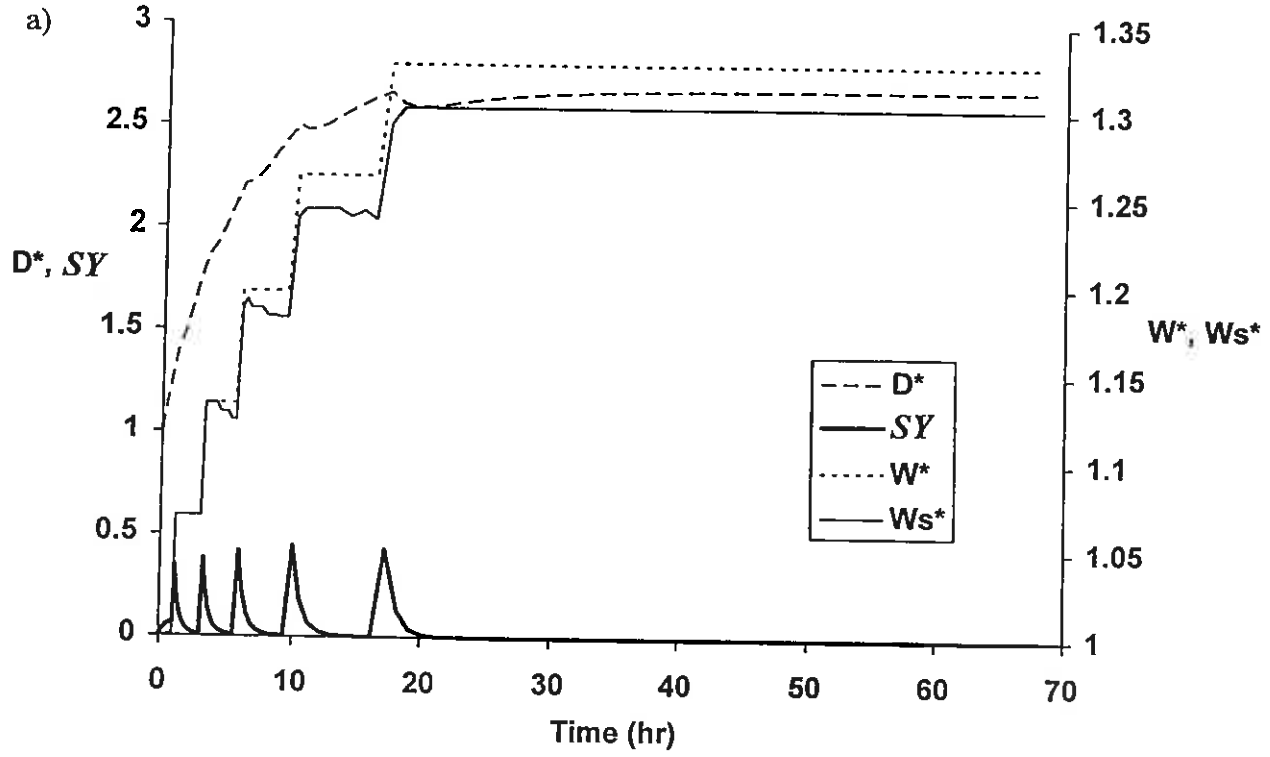

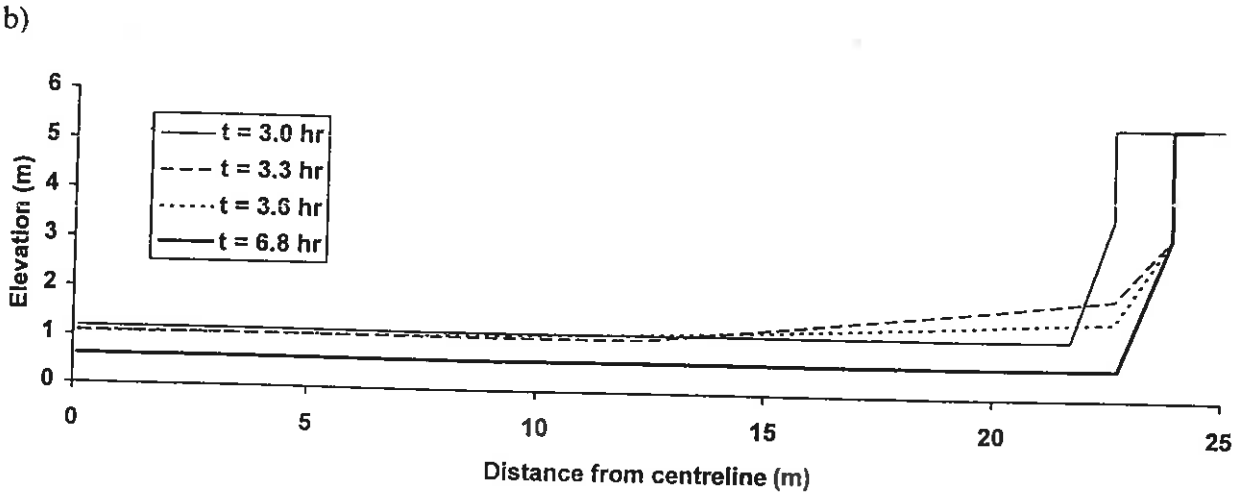

Figure 7: Model output for a simulation with $E = 0.06$; a) temporal variations in dimensionless channel depth, channel width and water surface width, and mean transverse bed slope; and b) sequence of morphological change.

a)

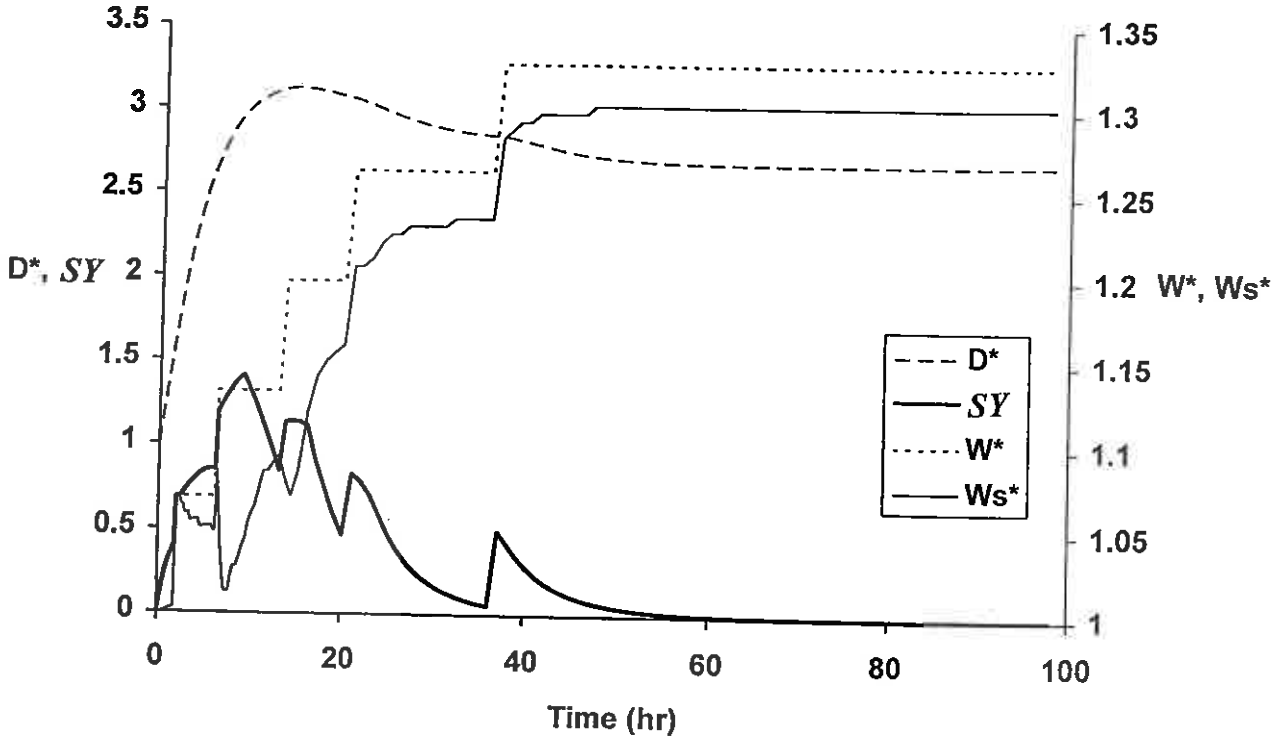

b)

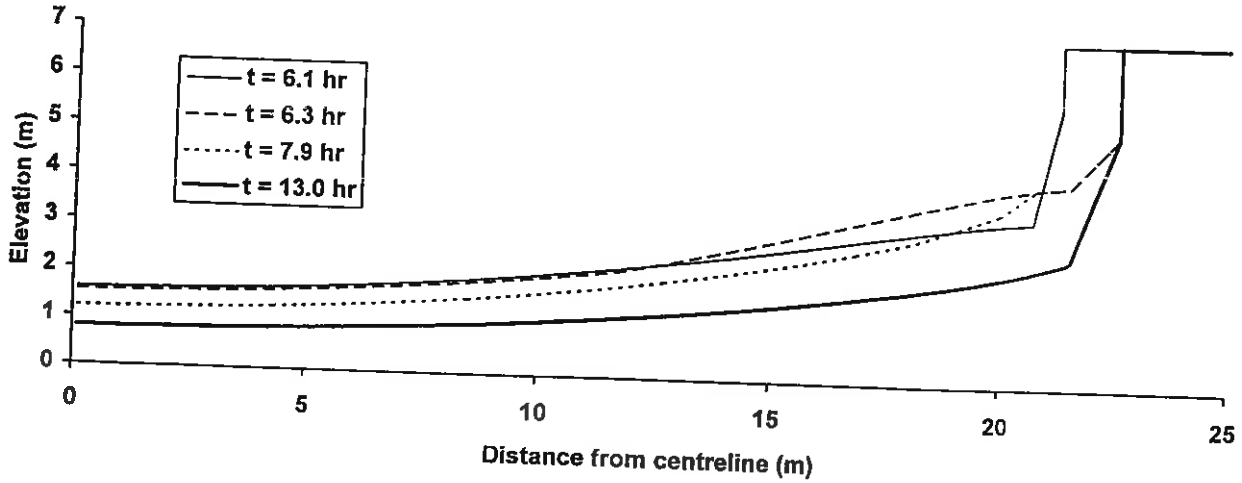

Figure 8: Model output for a simulation with $E = 0.004$; a) temporal variations in dimensionless channel depth, channel width and water surface width, and mean transverse bed slope; and b) sequence of morphological change.

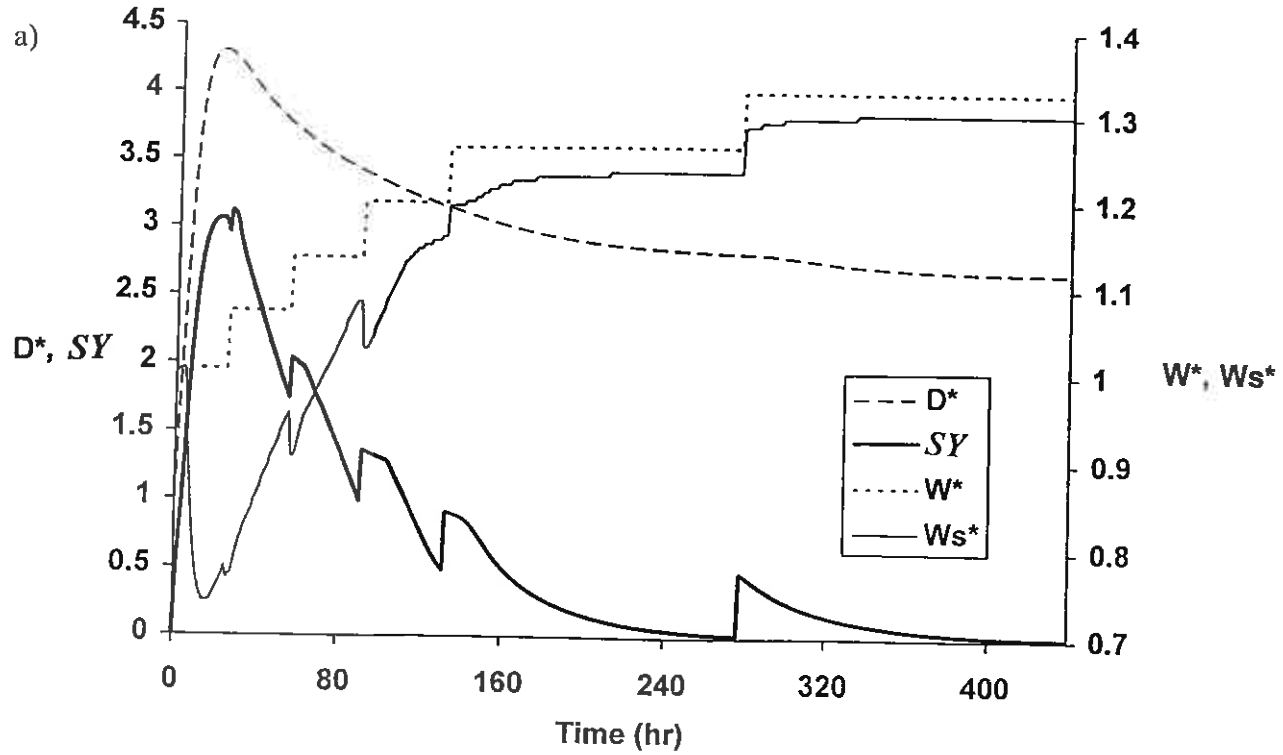

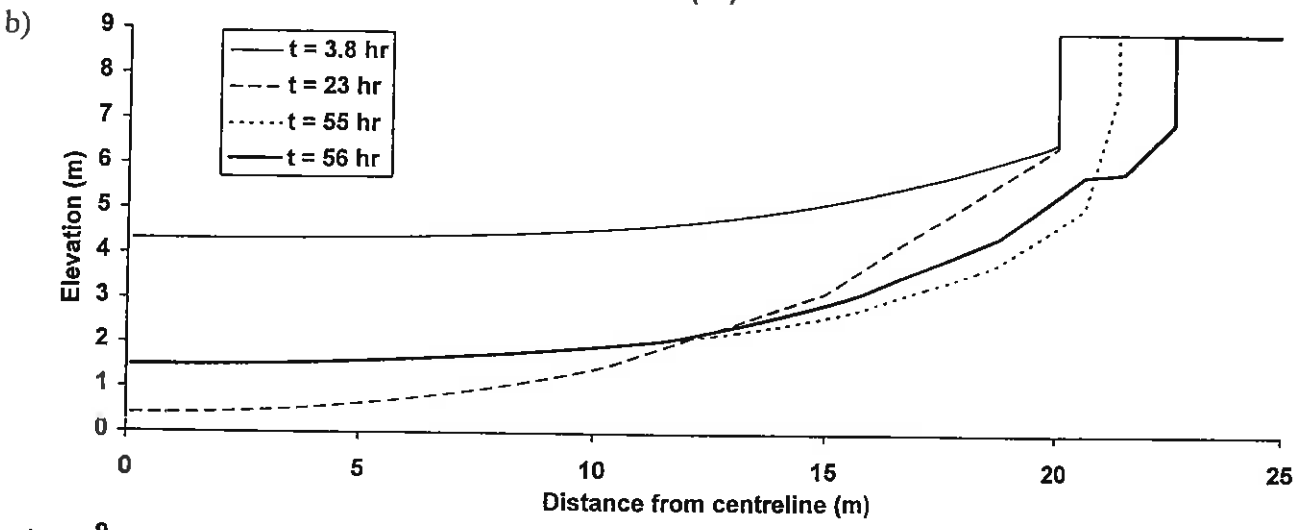

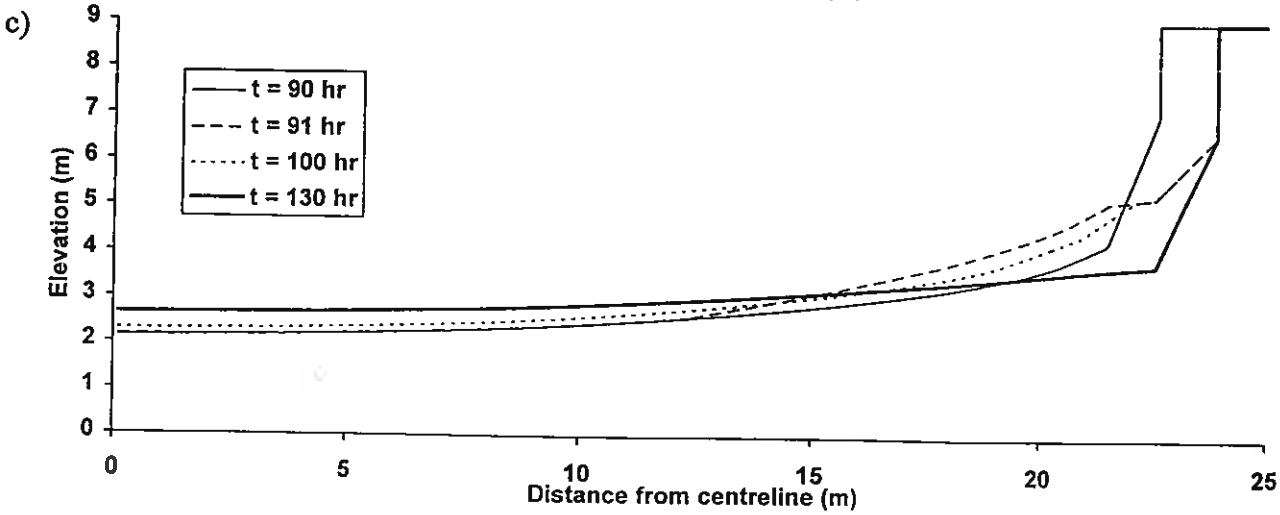

Figure 9: Model output for a simulation with E = 0.0006; a) temporal variations in dimensionless channel depth, channel width and water surface width, and mean transverse bed slope; b) and c) sequences of morphological change.

Figures 7a and 7b show the results of a simulation with $E = 0.06$. The increased effectiveness of cross-stream transport in this simulation promotes rapid lateral redistribution of sediment from the bank toe towards the channel centreline. As a result, the channel bed has a very low transverse slope that is quickly re-established after the deposition of sediment at the toe of the cohesive bank following its failure. Because cross-stream sediment transport inhibits the development of a significant lateral bed slope, the period of declining channel depth after the initial stages of the simulation shown in Figure 4a is not evident in Figure 7a. In addition, redistribution of the sediment deposited after a bank failure is so rapid that the channel centreline depth declines briefly before ongoing removal of material from the section promotes continued centreline incision.

Figures 8a and 8b show the results of a simulation with $E = 0.004$. In some respects the results of this simulation are similar to those shown in Figures 4 and 5. However, in this simulation cross-stream transport rates are slightly less effective than those in the default model run ($E = 0.006$). The result of this is that the lateral bed slope is marginally increased so that following the first failure of the cohesive bank (Figure 8b, $t = 6.3$ hr) the water surface drops below the level of the bank toe leaving a portion of the gravel bed exposed. Further evidence of this behaviour is provided by the reduction in the dimensionless water surface width in Figure 8a. Subsequently, lateral sediment transport moves sediment towards the channel centreline and promotes the development a steep transverse gravel slope at the channel edge (Figure 8b, $t = 7.9$ hr). When this slope exceeds the tangent of the angle of repose of the bed sediment the exposed gravel surface is trimmed by a series of small uncohesive failures. Ultimately, the gravel slope retreats to the toe of the cohesive bank which is then eroded vertically and horizontally in the usual manner.

Figures 9a to 9c show the results of a simulation with $E = 0.0006$. Very low cross-stream sediment transport rates in this simulation are unable to counteract the impacts of concentrated incision in the centre of the channel. This results in the development of a steep lateral bed slope so that the water surface falls below the level of the cohesive bank toe before the bank fails for the first time. The channel centreline depth reaches a maximum when the rate of sediment removal from the section begins to decline significantly ($t = 20$-30 hr). From this time onwards, lateral

sediment transport becomes more effective at reducing the transverse bed slope. As in the previous simulation, this promotes the development of a steep gravel slope at the edge of the water surface that is trimmed by a series of uncohesive failures. Gradually, sediment is transported away from the near bank region, the centreline channel bed rises, the lateral bed slope declines and the water surface begins to reoccupy the full width of the channel. These long-term trends in model variables are interrupted by a series of cohesive bank failures that temporarily re-establish the wedge of slumped material at the bank toe. In the first half of the simulation, while the transverse bed slope is significant, the material deposited by these cohesive bank failures may be exposed close to the bank (Figure 9c, t = 91 hr), resulting in a temporary reduction in water surface width (Figure 9a). As before, this exposed sediment wedge retreats towards the bank toe over time (Figure 9c, t = 100 hr).

The simulation results presented in Figures 7 to 9 illustrate the impact of changes in the effectiveness of cross-stream sediment transport upon the sequence of morphological change experienced within the section. Cross-stream sediment transport rates control the redistribution of sediment from the bank toe region to the channel centreline. Where cross-stream transport rates are high the transverse bed slope remains low throughout the simulation. As lateral transport rates decline, cross-stream bed slopes become steeper. At some threshold value of E, enhanced development of the transverse bed gradient causes the water surface to fall below the level of the cohesive bank toe. This leads to the exposure of a portion of the gravel bed. Cross-stream sediment transport acts to steepen the face of this exposed gravel surface and causes it to retreat in response to a series of uncohesive failures. Ultimately, these failures undermine the toe of the cohesive bank which in turn also fails, potentially re-establishing a wedge of exposed failure material.

The features of the model performance outlined in the last section have been related to variations in the value of the parameter E. In fact, the sequence of morphological changes during a simulation is controlled by the rate of cross-stream sediment transport relative to the rate of sediment removal from the section. The latter is a product of the erosion decay constant in equation (17). Figure 10 illustrates these relationships between cross-section shape and the ratio of the channel degradation decay coefficient to the lateral sediment transport rate (Γ/E).

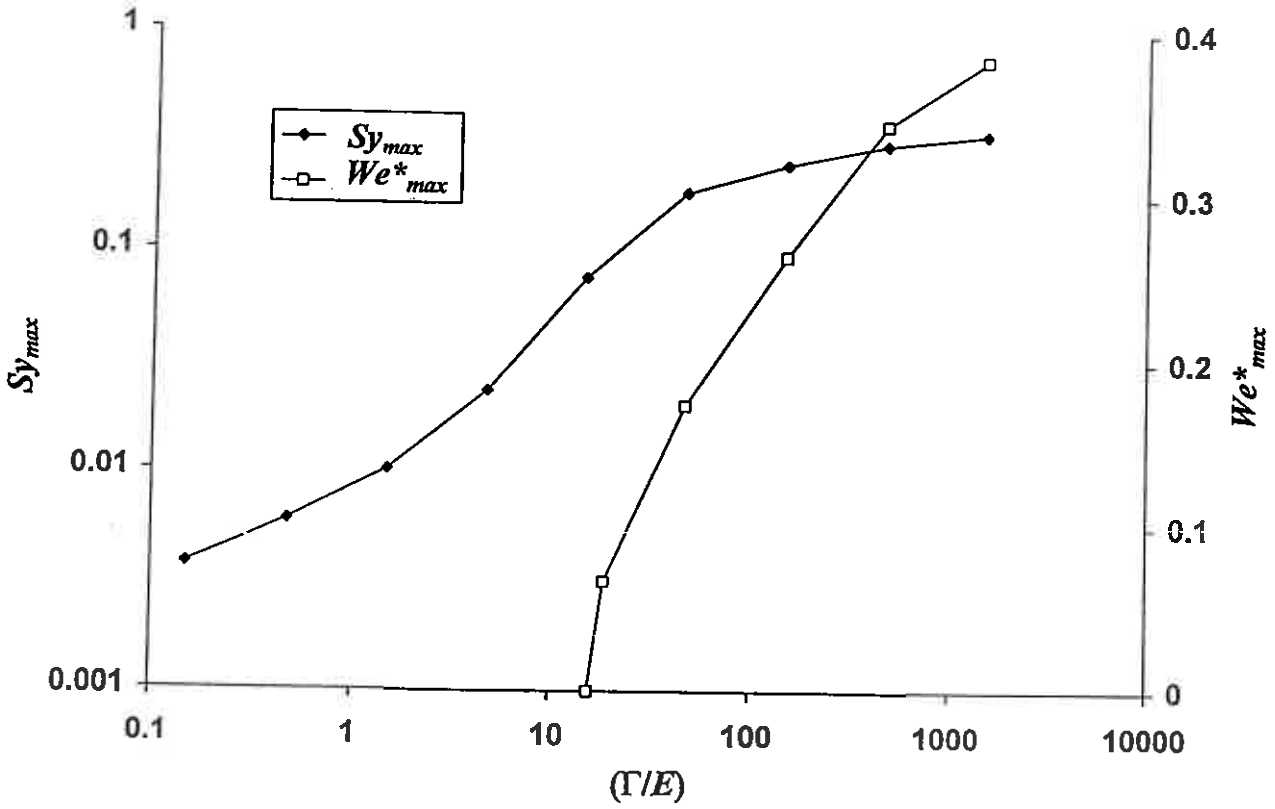

Figure 10: Relationships between the ratio of the channel erosion decay coefficient to the cross-stream sediment transport rate and both the maximum mean transverse bed slope and maximum dimensionless width of exposed channel bed.

In this figure, Sy_{max} is the maximum value over the course of the simulation of the section-averaged time-averaged transverse bed slope, and We^*_{max} is the maximum value over the course of the simulation of the proportion of the gravel bed exposed above the water surface. Figure 10 shows that as the ratio of the erosion decay constant to the lateral sediment transport effectiveness increases both the mean transverse bed slope and, above a threshold value of this ratio, the width of the exposed gravel surface also increase. These observations are examined further below.

DISCUSSION

The simulation model presented here brings together elements from a number of previous models of bank erosion and sediment transport to give a more complete representation of the process-form interrelationships that control the evolution of straight degrading river channels. The model provides a useful tool for examining the factors controlling fluvial erosion processes and temporal sequences of morphological change during bed degradation. However, comparison of the results of the simulations outlined above with field observations of degradation processes in natural channels suggests that the model could benefit considerably from a number of modifications.

Model realism could be improved by employing a flow-frequency distribution rather than a single formative discharge. This would make it possible to consider predicted rates of morphological change in real time. In addition, it would provide a more realistic representation of extreme flood events.

In its current form the model uses a single parameter to describe the size of the channel bed sediment (i.e. the bed D_{50}). Furthermore, this parameter is held constant throughout each simulation. In reality, bed degradation is generally associated with preferential entrainment of the finer grain size fractions and the development of a coarse armour layer (Dietrich *et al.*, 1989). This may reduce rates of bed incision significantly and cause increased rates of channel widening. This behaviour could be included in the model by employing a number of grain sizes and allowing the proportion of the bed material in each fraction to vary over the course of a simulation.

The treatment within the model of failure block deposition following bank collapse represents a significant improvement over previous models of bank erosion, and appears to be an essential component of any scheme that seeks to simulate channel degradation in a realistic manner. However, the approach to this problem adopted here could be improved in a number of ways. Bank failure may occur by a range of processes not accounted for in the model including rotational slips and cantilever failure (c.f. Thorne, 1982). Furthermore, the fate of the failure block following bank collapse may differ significantly from that postulated here. The model assumes that the failed bank material is incorporated within the gravel bed, and may subsequently be treated as non-cohesive sediment. The fine fraction of the failure block might be considered to be removed in suspension, by using a value of P in equation (39) of less than one. However, in natural channels failed bank material may remain in the channel at the bank toe as a cohesive block, possibly in association with intact vegetation. Incorporation of this phenomena within the model could be achieved by representing the failure block and the gravel below it as separate bed layers with different properties.

In addition to the model refinements outlined above, a number of other process-form interactions have been omitted from the model with potentially significant implications. Simon (1989) and Hupp (1992) describe a six stage model of the morphological development of stream channels in Western Tennessee, USA following river channelisation. Bed degradation and river widening by mass failure occur in response to increases in sediment transport capacity following the steepening of channel gradients. This phase of channel erosion is subsequently replaced by a period of aggradation and restabilisation of riparian vegetation. Accretion of fine sediment at the channel margins is accompanied by recolonisation of depositional surfaces. Over time these restabilised surfaces extend both upslope and downslope. Clearly, in certain situations the inclusion of these processes within the simulation model presented here would have a significant impact upon predicted equilibrium channel morphology following degradation. Where cross-stream sediment transport rates are high relative to rates of bed degradation, removal of failed bank material is rapid and transverse bed slopes are low. In contrast, where cross-stream transport rates are low compared to net channel erosion a significant lateral bed slope develops

and a portion of the channel's gravel bed may become exposed above the water surface. In the natural environment, overbank deposition of suspended sediment and growth of vegetation may subsequently increase the stability of such an exposed gravel surface (Gray and Leiser, 1982) leading to the creation of a second, lower bank with cohesive properties. This bank may in turn retreat by mass failure until the original cohesive bank is again undermined. Alternatively, the new cohesive bank may stabilise to leave a compound channel cross-section composed of an trapezoidal channel bordered by an inclined floodplain surface that extends laterally to the base of the former channel bank. Clearly, the combination of rapid bed incision concentrated around the channel centreline, exposure of the near bank gravel bed and stabilisation of this former bed surface, by the accretion of fine sediment and growth of vegetation, may provide a mechanism capable of promoting the sequences of channel incision and narrowing that have been observed in field situations (e.g. James, 1991).

SUMMARY

A theoretical model has been presented that is capable of simulating the response of a straight river channel with a gravel bed and cohesive banks to a phase of rapid or substantial bed degradation. The model couples elements from a number of previous numerical schemes to give a more complete treatment of flow hydraulics, bed degradation, cross-stream sediment transport and the failure of both cohesive banks and non-cohesive bed slopes. This enables a detailed examination of the temporal sequence of channel incision, bank failure, deposition of failed bank material and removal of sediment from the bank toe by cross-stream and downstream transport.

Analysis of the model's performance indicates that variations in the magnitude and frequency of simulated bank failures are controlled by the properties of the bank material and the geometry of the cohesive bank and failure block. In addition, low magnitude failures occur with increased frequency and are more effective agents of channel widening than high magnitude, low frequency failures.

The sequence of morphological changes within a section during a simulation are controlled largely by the relative rates of bed degradation and cross-stream sediment transport. Rapid lateral sediment transport promotes low transverse bed

slopes. Conversely, weak cross-stream transport results in the development of a steep transverse bed slope and exposure of a portion of the gravel bed adjacent to the cohesive bank. Further modification of the model presented here to include variations in flow discharge, deposition of fine sediment in shallow flows near the channel margins and colonisation of accreted gravel surfaces by vegetation could lead to improved model predictions of post-degradational equilibrium channel morphology.

ACKNOWLEDGEMENTS

Preliminary work on the simulation model presented in this paper was undertaken while the author was engaged in postdoctoral research funded by a Leeds University, School of Geography research initiative (SUPERSLUGS). Model development and testing were completed while the author was in receipt of a NERC Postdoctoral Research Fellowship (Grant number GT5/95/FS/7).

REFERENCES

Arulanandan, k., Gillogley, E. and Tully, R. 1980. Development of a quantitative method to predict critical shear stress and rate of erosion of natural undisturbed cohesive soils, *Report GL-80-5*, US Army Engineers, Waterways Experiment Station, Vicksburg, Miss.

Bagnold, R.A. 1980. An empirical correlation of bedload transport rates in flumes and natural rivers. *Proceedings of the Royal Society. London. Ser A*, 372, 453-473.

Brookes, A. 1985. River channelisation; traditional engineering methods, physical consequences and alternative practices, *Progress in Physical Geography*, 9, 44-73.

Burrin, P.J. 1985. Holocene alluviation in Southeast England and some implications for palaeohydrological studies, *Earth Surface Processes and Landforms*, 10, 257-271.

Chang, H.H. 1982. Mathematical models for erodible channels, *Journal of Hydraulic Engineering*, 106, 1132-1139.

Dawdy, D.R. and Vanoni, V.A. 1986. Modeling alluvial channels, *Water Resources Research*, 9, 71S-81S.

Dietrich, W.E., Kirchner, J.W., Ikeda, H. and Iseya, F. 1989. Sediment supply and the development of a coarse surface layer in gravel-bedded rivers, *Nature*, 340, 215-217.

Erskine, W.D. 1992. Channel response to large-scale river training works; Hunter River, Australia, *Regulated Rivers: Research and Management*, 7, 261-278.

Ferguson, R.I. 1994. Critical discharge for entrainment of poorly sorted gravel, *Earth Surface Processes and Landforms*, 19, 179-186.

Graf, W.L. 1977. The rate law in fluvial geomorphology, *American Journal of Science*, 277, 178-191.

Gray, D.H. and Leiser, A.T. 1982. *Biotechnical slope protection and erosion control*, Van Nostrand, Reinhold, New York.

Hickin, E.J. 1983. River channel changes: retrospect and prospect, *Spec. Publs. int. Ass. Sediment.*, 6, 61-83.

Hupp, C.R. 1992. Riparian vegetation recovery patterns following stream channelization: A geomorphic perspective, *Ecology*, 73, 1209-1226

James, A.L. 1991. Incision and morphological response of an alluvial channel recovering from hydraulic mining sediment, *Geological Society of America Bulletin*, 103, 723-736.

Kikkawa, H., Ikeda, S. and Kitagawa, A. 1976. Flow and bed topography in curved open channels, *Journal of Hydraulic Engineering*, 102, 1327-1342.

Knighton, A.D. 1989. River adjustment to changes in sediment load: the effects of tin mining on the Ringarooma River, Tasmania, 1875-1984, *Earth Surface Processes and Landforms*, 14, 333-359.

Knox, J.C. 1983. Responses of river systems to Holocene climates. In: H.E. Wright, Jr. (Ed), *Late Quaternary Environments of the United States*, University of Minnesota Press, Minneapolis, 26-41.

Leckie, D.A. 1994. Canterbury Plains, New Zealand - Implications for sequence stratigraphic models, *AAPG Bulletin*, 78, 1240-1256.

Lewin, J., Macklin, M.G. and Newson, M.D. 1988. Regime theory and environmental change - irreconcilable concepts? In: W.R. White (Ed). *International Conference on River Regime*, 431-445.

Mosselman, E. 1995. A review of mathematical models of river planform changes, *Earth Surface Processes and Landforms*, 20, 661-670.

Nicholas, A.P., Ashworth, P.J., Kirkby, M.J., Macklin, M.G. and Murray, T. 1995. Sediment slugs: Large-scale fluctuations in fluvial sediment transport rates and storage volumes, *Progress in Physical Geography*, 19, 500-519.

Osman, A.M. and Thorne, C.R. 1988. Riverbank stability analysis. I: Theory, *Journal of Hydraulic Engineering*, 114, 134-150.

Park, C.C. 1977. Man-induced changes in stream channel capacity. In: K.J. Gregory (Ed), *River Channel Changes*, Wiley, Chichester, 121-144.

Parker, G. 1978. Self-formed straight rivers with equilibrium banks and mobile bed, 2. The gravel river, *Journal of Fluid Mechanics*, 89, 127-146.

Parker, G. 1983. Discussion of 'lateral bed load transport on side slopes', *Journal of Hydraulic Engineering*, 109, 197-199.

Parker, G. 1990. Surface-based bedload transport relation for gravel rivers, *Journal of Hydraulic Research*, 28, 417-436.

Petts, G.E. 1979. Complex response of river channel morphology subsequent to reservoir construction, *Progress in Physical Geography*, 3, 329-362.

Pickup, G. 1976. Simulation modelling of river channel erosion. In: K.J. Gregory (Ed). *River Channel Changes*. Wiley, Chichester, 47-60.

Pizzuto, J.E. 1990. Numerical simulation of gravel river widening, *Water Resources Research*, 26, 1971-1980.

Rasid, H. 1979. The effects of regime regulation by the Gardiner Dam on downstream geomorphic processes in the South Saskatchewan River, *Canadian Geographer*, 23, 140-158.

Schumm, S.A. 1969. River metamorphosis, *Journal of the Hydraulics Division, ASCE,* 95, 255-273.

Schumm, S.A. and Lichty, R.W. 1965. Time, space and causality in geomorphology, *American Journal of Science*, 263, 110-119.

Shiono, K. and Knight, D.W. 1991. Turbulent open-channel flows with variable depth across the channel, *Journal of Fluid Mechanics*, 222, 617-646.

Simon, A. 1989. A model of channel response in disturbed alluvial channels, *Earth Surface Processes and Landforms*, 14, 11-26.

Thorne, C.R. 1982. Processes and mechanisms of river bank erosion. In: R.D. Hey, J.C. Bathhurst, and C.R. Thorne (Eds). *Gravel-bed Rivers, Fluvial Processes, Engineering and Management*. Wiley, Chichester, 227-271.

Thorne, C.R. and Abt, S.R. 1993. Analysis of riverbank instability due to toe scour and lateral erosion, *Earth Surface Processes and Lanforms*, 18, 835-843.

Thorne, C.R. and Osman, A.M. 1988. Riverbank stability analysis. II: Applications, *Journal of Hydraulic Engineering*, 114, 151-172.

Whitlow, J.R. and Gregory, K.J. 1989. Changes in urban stream channels in Zimbabwe. *Regulated Rivers: Research and Management*, 4, 27-42.